Treatment of Supersonic Flows with Embedded Subsonic Regions

Vijaya Shankar* and Kuo-Yen Szema†
Rockwell International Science Center, Thousand Oaks, California

and

Stanley Osher‡
University of California, Los Angeles, California

A nonlinear method based on the full potential equation in conservation form, cast in an arbitrary coordinate system, has been developed to treat predominantly supersonic flows with embedded subsonic regions. This type of flow field occurs frequently near the fuselage/canopy junction area and wing leading-edge regions for a moderately swept fighter configuration. The method uses the theory of characteristics to accurately monitor the type-dependent flowfield. A conservative switching scheme is developed to handle the transition from the supersonic marching algorithm to a subsonic relaxation procedure, and vice versa. An implicit approximate factorization scheme is employed to solve the finite differenced equation. Results are shown for a few configurations, including a wing/body/wake realistic fighter model having embedded subsonic regions.

I. Introduction

NONLINEAR aerodynamic prediction methods based on the full potential equation are used regularly for treating transonic[1,2] and supersonic[3-5] flows over realistic wing/body configurations. The transonic algorithms[1,2] are designed to treat predominantly subsonic flows with pockets of supersonic regions bounded by sonic lines and shocks. The supersonic methods[3-5] are based on a marching concept and require the flow to remain supersonic in a given marching direction. Once the marching direction velocity becomes subsonic, the domain of dependence changes and a pure marching scheme[3-5] will violate the rules of characteristic signal propagation. The possibility of a marching velocity becoming subsonic in a supersonic flow is great, especially for low supersonic freestream Mach number flows ($M_\infty = 1.3 \sim 1.7$) over moderately swept fighter-like configurations (sweep angle $\Lambda = 45 \sim 50$ deg) and over forebody shapes having a sizeable fuselage/canopy junction region. *There is a strong need to construct a supersonic marching computer program that has built-in logics to detect and treat the embedded subsonic regions.*

The method of Ref. 5 is based on the characteristic theory of signal propagation and uses a generalized, nonorthogonal, curvilinear coordinate system. Compared to other nonlinear supersonic methods,[3] the method of Ref. 5 has no restrictions (limitations of the full potential theory hold) on its applicability to complex geometries and intricate shocked flowfields. It is a conservative formulation and uses numerical mapping techniques to generate the body-fitted system. The purpose of this paper is to describe an extension to the methodology of Ref. 5 to include the treatment of embedded subsonic regions in a supersonic flow.

The paper describes the characteristic theory involved in determining the condition for a marching direction to exist. Once that condition is violated, the marching scheme is transitioned to a relaxation scheme through a conservative switching operator. For marching condition violation, the total velocity q does not have to be subsonic. Even for a supersonic total velocity q, if the component in the marching direction is subsonic, a relaxation scheme is required. In order to properly produce the necessary artificial viscosity through density biasing, the paper defines two situations: 1) the total velocity q is supersonic, but the marching direction component is subsonic [defined as marching subsonic region (MSR)]; and 2) the total velocity q is subsonic [termed as total subsonic region (TSR)].

Results are presented for a few configurations that exhibit either the MSR or both the MSR and TSR flowfield. The paper also presents results from a wake model applied to a realistic wing/body fighter configuration.

The Appendix describes a flux biasing concept that will supersede the density biasing procedures currently in use.

The methodology of this paper is not restricted to the full potential equation alone. Currently, similar marching/relaxation methods are under development at Rockwell for application in parabolized Navier-Stokes (PNS) codes to treat the embedded subsonic regions or streamwise separated flows without having to use a time-dependent Navier-Stokes program.

II. Equation and Characteristic Theory

The conservative full potential equation cast in an arbitrary coordinate system defined by $\zeta = \zeta(x, y, z)$, $\eta = \eta(x, y, z)$, and $\xi = \xi(x, y, z)$, takes the form

$$\left(\rho\frac{U}{J}\right)_\zeta + \left(\rho\frac{V}{J}\right)_\eta + \left(\rho\frac{W}{J}\right)_\xi = 0 \tag{1}$$

where U, V, and W are the contravariant velocity components. Introducing the following notation for convenience:

$$U = U_1, \quad V = U_2, \quad W = U_3$$

$$x = x_1, \quad y = x_2, \quad z = x_3$$

$$\zeta = X_1, \quad \eta = X_2, \quad \xi = X_3$$

Received June 30, 1983; presented as Paper 83-1887 at the AIAA Computational Fluid Dynamics Meeting, Danvers, Mass., July 13-15, 1983; revision received March 19, 1984.

*Manager, Computational Fluid Dynamics Group. Associate Fellow AIAA.

†Member, Technical Staff. Member AIAA.

‡Professor, Department of Mathematics. Member AIAA.

the contravariant velocities and density are given by

$$U_i = \sum_{j=1}^{3} a_{ij}\phi_{X_j} \qquad i = 1, 2, 3$$

$$a_{ij} = \sum_{k=1}^{3} \frac{\partial X_i}{\partial x_k}\frac{\partial X_j}{\partial x_k} \qquad \begin{matrix} i = 1,2,3 \\ j = 1,2,3 \end{matrix} \quad \text{(transformation metrics)}$$

$$\rho = \left[1 - \left(\frac{\gamma - 1}{2}\right) M_\infty^2 \{ U\phi_\zeta + V\phi_\eta + W\phi_\xi - 1 \}\right]^{1/(\gamma-1)}$$

$$a = \text{speed of sound} = \sqrt{\rho^{(\gamma-1)}/M_\infty^2} \tag{2}$$

The Jacobian of the transformation J is represented by

$$J = \frac{\partial(\zeta, \eta, \xi)}{\partial(x, y, z)} = \begin{bmatrix} \zeta_x & \zeta_y & \zeta_z \\ \eta_x & \eta_y & \eta_z \\ \xi_x & \xi_y & \xi_z \end{bmatrix} \tag{3}$$

Equation (1) is in terms of a general coordinate system (ζ, η, ξ) and can accommodate any kind of mapping procedure, either analytical (conformal mapping) or numerical. The nature of Eq. (1) can be analyzed by studying the eigenvalue system of Eq. (1). Combining the irrotationality condition in the (ζ, η) and (ζ, ξ) plane and Eq. (1), one can write the following matrix equation:

$$Af_\zeta + Bf_\eta + Cf_\xi = 0 \tag{4}$$

where

$$A = \begin{bmatrix} \frac{1}{J}(\rho U)_{\phi_\zeta} & \frac{1}{J}(\rho U)_{\phi_\eta} & \frac{1}{J}(\rho U)_{\phi_\xi} \\ 0 & 1 & 0 \\ 0 & 0 & 1 \end{bmatrix}$$

$$B = \begin{bmatrix} \frac{1}{J}(\rho V)_{\phi_\zeta} & \frac{1}{J}(\rho V)_{\phi_\eta} & \frac{1}{J}(\rho V)_{\phi_\xi} \\ -1 & 0 & 0 \\ 0 & 0 & 0 \end{bmatrix}$$

$$C = \begin{bmatrix} \frac{1}{J}(\rho W)_{\phi_\zeta} & \frac{1}{J}(\rho W)_{\phi_\eta} & \frac{1}{J}(\rho W)_{\phi_\xi} \\ 0 & 0 & 0 \\ -1 & 0 & 0 \end{bmatrix}$$

$$f = \begin{bmatrix} \phi_\zeta \\ \phi_\eta \\ \phi_\xi \end{bmatrix}$$

The subscripts in Eq. (4) denote differentiation with respect to that variable.

The matrices A, B, and C appearing in Eq. (4) can now be analyzed to determine the character of that equation. In general, the following is true:

1) Equation (4) is *elliptic in the ζ direction* if the matrix $A^{-1}(\alpha B + \beta C)$ has complex eigenvalues for all combinations of α and β such that $\alpha^2 + \beta^2 = 1$.

2) Equation (4) is *hyperbolic in the ζ direction* if $A^{-1}(\alpha B + \beta C)$ has real eigenvalues for all α and β satisfying $\alpha^2 + \beta^2 = 1$.

The eigenvalue structure of $A^{-1}(\alpha B + \beta C)$ can be obtained by setting the determinant

$$|\alpha B + \beta C - \lambda A| = 0 \qquad (\text{assuming } A^{-1} \text{ exists}) \tag{5}$$

Substituting for A, B, and C from Eq. (4), the eigenvalues of Eq. (5) are given by solving the quadratic

$$-\lambda^2(\rho U)_{\phi_\zeta} + \lambda\left[\alpha(\rho V)_{\phi_\zeta} + B(\rho W)_{\phi_\zeta} + \alpha(\rho U)_{\phi_\eta} + \alpha(\rho U)_{\phi_\xi}\right] - \left\{\alpha^2(\rho V)_{\phi_\eta} + \beta^2(\rho W)_{\phi_\xi} + \alpha\beta\left[(\rho W)_{\phi_\eta} + (\rho V)_{\phi_\xi}\right]\right\} = 0 \tag{6}$$

Representing Eq. (6) in the form

$$\bar{A}\lambda^2 + \bar{B}\lambda + \bar{C} = 0 \tag{7}$$

the discriminant $(\bar{B}^2 - 4\bar{A}\bar{C})$ determines the character of Eq. (4):

1) If $(\bar{B}^2 - 4\bar{A}\bar{C})$ remains *positive* for all α and β satisfying $\alpha^2 + \beta^2 = 1$, then the eigenvalues of Eq. (4) are real and direction ζ is hyperbolic (marching scheme is valid).

2) If $(\bar{B}^2 - 4\bar{A}\bar{C})$ is *negative*, then the eigenvalues of Eq. (4) are complex and direction ζ is elliptic (requires a relaxation method).

To analyze when the eigenvalue solutions of Eq. (6) are real and when complex, the discriminant $(\bar{B}^2 - 4\bar{A}\bar{C})$ is rewritten in the following form using Eq. (2):

$$\bar{B}^2 - 4\bar{A}\bar{C} = \alpha^2\left[\left(a_{21} - \frac{UV}{a^2}\right)^2 - \left(a_{11} - \frac{U^2}{a^2}\right)\left(a_{22} - \frac{V^2}{a^2}\right)\right] + 2\alpha\beta\left[\left(a_{21} - \frac{UV}{a^2}\right)\left(a_{31} - \frac{UW}{a^2}\right) - \left(a_{11} - \frac{U^2}{a^2}\right)\left(a_{23} - \frac{VW}{a^2}\right)\right] + \beta^2\left[\left(a_{31} - \frac{UW}{a^2}\right)^2 - \left(a_{11} - \frac{U^2}{a^2}\right)\left(a_{33} - \frac{W^2}{a^2}\right)\right] \tag{8}$$

Using the properties of a positive definite quadratic form and the Schwarz inequality $(a_{ii}a_{jj} > a_{ij}^2)$, Eq. (8) can be shown to have the following results:

1) $(\bar{B}^2 - 4\bar{A}\bar{C})$ is positive if $[a_{11} - (U^2/a^2)]$ is less than zero. Then the ζ direction is hyperbolic (the marching algorithm of Ref. 5 is valid).

2) $(\bar{B}^2 - 4\bar{A}\bar{C})$ is negative if $[a_{11} - (U^2/a^2)]$ is greater than zero. Then the ζ direction is elliptic (requires a relaxation scheme).

Physical Interpretation

The physical interpretation of these results from the characteristic theory is illustrated in Fig. 1. Let q be the total velocity. The projection of q in the direction normal to the ζ = constant surface is given by

$$\vec{q} \cdot \vec{n} = (u\hat{i} + v\hat{j} + w\hat{k}) \frac{(\zeta_x\hat{i} + \zeta_y\hat{j} + \zeta_z\hat{k})}{\zeta_x^2 + \zeta_y^2 + \zeta_z^2} = U/\sqrt{a_{11}} \tag{9}$$

where u, v, and w are the Cartesian velocities and $\vec{n}$ the normal to the ζ = constant plane. Figure 1a shows the case when $U/\sqrt{a_{11}}$ is greater than the speed of sound $\{[a_{11} - (U^2/a^2)] < 0\}$. For this case, the characteristic cone of influence is behind the ζ = constant plane and marching along ζ is valid. Figure 1b illustrates the case for the $q > a$, but for the $U/\sqrt{a_{11}} < a$ situation, $[a_{11} - (U^2/a^2)] > 0$. For this case, a part of the characteristic cone of influence lies forward of the ζ = constant plane and marching along ζ is not possible. This case (Fig. 1b) is termed marching subsonic region (MSR) in this paper. Figure 1c shows the case when $q < a$ and $U/\sqrt{a_{11}} < a$, $[a_{11} - (U^2/a^2)] > 0$. This represents a pure subsonic flow and marching along ζ is not possible. This case is termed total subsonic region (TSR). For cases represented in Figs. 1b and 1c, a relaxation algorithm is required.

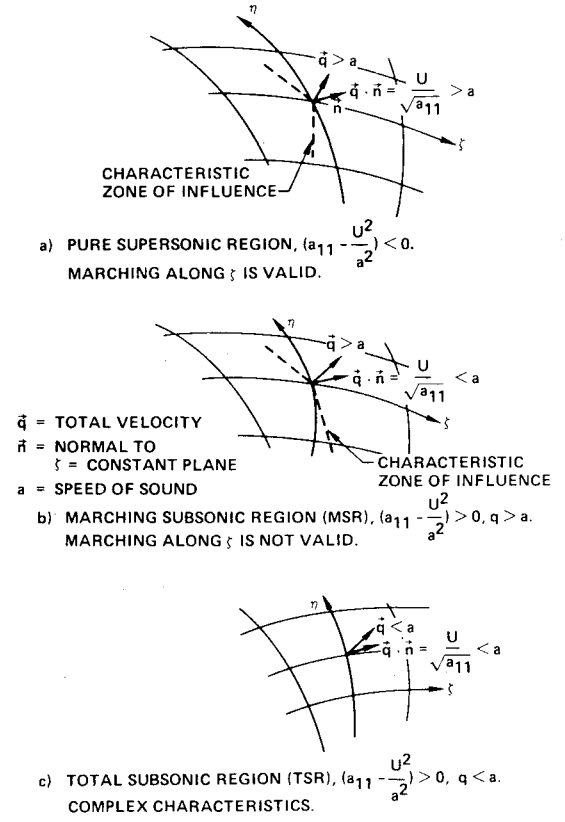

Fig. 1 Role of characteristics in defining supersonic region, marching subsonic region (MSR), and total subsonic region (TSR).

III. Numerical Method

Figure 2 shows the schematic of a fuselage/canopy forebody geometry with an embedded MSR and TSR present in a supersonic flow. To solve this problem, the marching scheme of Ref. 5 will be used when $[a_{11} - (U^2/a^2)]$ is negative and a relaxation scheme when $[a_{11} - (U^2/a^2)]$ is positive. First, march from the nose up to the plane denoted by (A-B) in Fig. 2, using the method of Ref. 5. Then, between (A-B) and (C-D), which embed the subsonic bubble (MSR and TSR), use a relaxation scheme and iterate until the subsonic bubble is fully captured. Then, resume the marching scheme from the plane (C-D), downstream of the body.

The purpose of this paper is to present a conservative algorithm that will automatically switch from a pure marching scheme of Ref. 5 to a relaxation method at the onset of an MSR formation and revert to the marching procedure when the flow becomes fully supersonic again. The entire flowfield can be classified into three types with respect to the marching direction ζ:

1) At a grid point, the marching direction is *hyperbolic* and the total velocity q is supersonic, $[a_{11} - (U^2/a^2)] < 0$, $q > a$. This point will use the algorithm of Ref. 5.

2) At a grid point, the marching direction ζ is *elliptic*, $[a_{11} - (U^2/a^2)] > 0$, but the total velocity q is supersonic, $q > a$ (MSR). This point will be treated by a transonic operator with a built-in density biasing based on the magnitude of $[1 - (a^2/q^2)]$.

3) At a grid point, the direction ζ is *elliptic* and the total velocity q is *subsonic*, $q < a$ (TSR). This point will be treated by a subsonic central differenced operator.

Treatment of $(\partial/\partial\zeta)[\rho(U/J)]$ in Eq. (1)

Refer to the computational molecule in Fig. 3.

$$\frac{\partial}{\partial\zeta}\left(\rho\frac{U}{J}\right) = \underbrace{\theta_i \frac{\vec{\partial}}{\partial\zeta}\left(\rho\frac{U}{J}\right)_{i+1}}_{\text{supersonic}} + \underbrace{(1-\theta_{i+1})\frac{\vec{\partial}}{\partial\zeta}\left(\tilde{\rho}\frac{U}{J}\right)_{i+1}}_{\text{marching subsonic}} \quad (10)$$

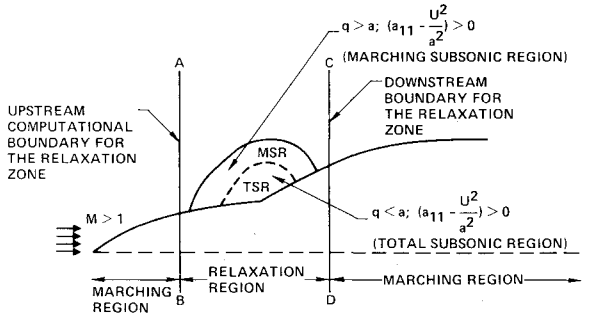

Fig. 2 Embedded subsonic bubble in a supersonic flow.

where

$\vec{\partial}$ refers to backward differencing

$\vec{\partial}$ refers to forward differencing

$$\theta_i = 1 \quad \text{if} \left(a_{11} - \frac{U^2}{a^2}\right) < 0$$

$$= 0 \quad \text{if} \left(a_{11} - \frac{U^2}{a^2}\right) > 0$$

In Eq. (10), the first term corresponds to the supersonic marching operator of Ref. 5 and the second term is the subsonic operator.

The backward difference operator in Eq. (10) is represented by

$$\frac{\vec{\partial}}{\partial\zeta}\left(\rho\frac{U}{J}\right)_{i+1} \doteq \frac{\vec{\partial}}{\partial\zeta}\rho_i\left[\left(a_{11} - \frac{U^2}{a^2}\right)\frac{\vec{\partial}}{\partial\zeta}\Delta\phi + \left(a_{12} - \frac{UV}{a^2}\right)\frac{\partial}{\partial\eta}\Delta\phi + \left(a_{13} - \frac{UW}{a^2}\right)\frac{\partial}{\partial\xi}\Delta\phi + U_i\right],$$

$$\Delta\phi = (\phi_{i+1} - \phi_i) \quad (11)$$

The term $(\partial/\partial\zeta)(\Delta\phi)$ is backward differenced. Reference 5 gives more details on this supersonic marching operator.

The forward difference operator in Eq. (10) is represented by

$$\frac{\vec{\partial}}{\partial\zeta}\left(\tilde{\rho}\frac{U}{J}\right)_{i+1} \doteq \frac{\vec{\partial}}{\partial\zeta}\left[\frac{\tilde{\rho}^{n+1}_{i+1}}{J}\left(a_{11}\overleftarrow{\phi}_\zeta + a_{12}\phi_\eta + a_{13}\phi_\xi\right)_{i+1}\right] \quad (12)$$

where

$$\tilde{\rho}^{n+1}_{i+1} = \rho^n_{i+1} - \nu\left(\rho^n_{i+1} - \rho^n_i\right), \qquad \text{for } U > 0$$

$$\nu = \max\left[0, 1 - \left(a^2/q^2\right)\right] \quad (13)$$

The superscript $n+1$ denotes the current relaxation cycle for a subsonic bubble calculation.

Note that in Eq. (12) the term ϕ_ζ is backward differenced such that $(\vec{\partial}/\partial\zeta)(\tilde{\rho}/J)a_{11}\overleftarrow{\phi}_\zeta$ will provide the central differencing needed for an elliptic (subsonic) point. The density biasing [Eq. (13)] is activated only when the total velocity q is greater than the speed of sound a. This will take place when a grid point is in the region denoted by MSR in Fig. 2. When $q < a$ (the TSR in Fig. 2), the density is not biased and the generation of artificial viscosity is turned off. The ϕ derivatives in Eq. (13) can be rewritten in terms of $\Delta\phi$, just as in Eq. (11).

Equation (10) can also be interpreted as

$$\frac{\partial}{\partial\zeta}\left(\rho\frac{U}{J}\right) = \underbrace{\frac{\vec{\partial}}{\partial\zeta}\left(\rho\frac{U}{J}\right)_{i+1}}_{\text{elliptic operator}} - \underbrace{\Delta\zeta\frac{\vec{\partial}}{\partial\zeta}\theta_{i+1}\frac{\vec{\partial}}{\partial\zeta}\left(\rho\frac{U}{J}\right)_{i+2}}_{\text{flux biasing to produce the artificial viscosity}} \quad (14)$$

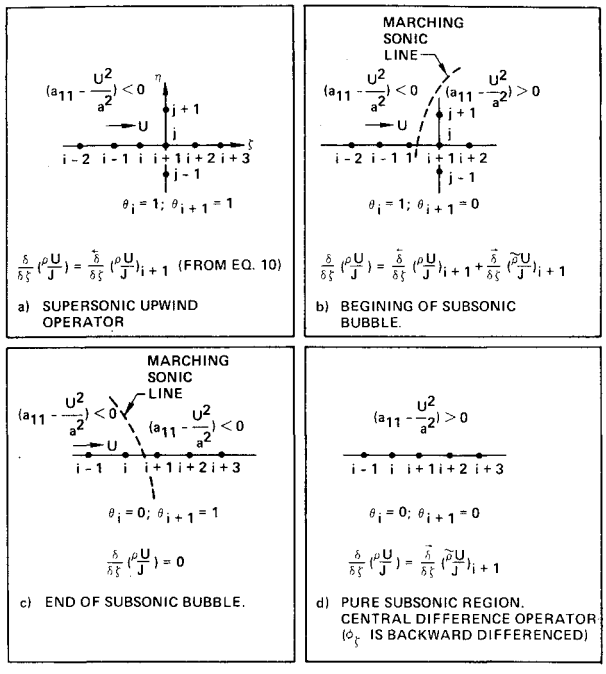

Fig. 3 Conservative type-dependent switching scheme for the treatment of subsonic bubble in a supersonic flow.

Figure 3 illustrates various possibilities that can be handled by Eq (10). It has both the shock point operator and the sonic operator required to treat the type-dependent flow. The only issue that philosophically affects the concept of a conservative scheme is that the definition of ρU for a supersonic operator in Eq. (11) is different from the definition for the subsonic operator of Eq. (12).

The evaluation of the subsonic operator in Eq. (12) requires velocity potential ϕ values at $i+1$ and $i+2$ planes from the previous n relaxation cycle to compute the density. The section on initial and boundary conditions below prescribes a method to start the first relaxation cycle of the subsonic bubble calculation.

Treatment of $(\partial/\partial\eta)[\rho(V/J)]$ in Eq. (1)

Referring to the Fig. 3a molecule,

$$\frac{\partial}{\partial\eta}\left(\rho\frac{V}{J}\right) = \theta_{i+1}\underbrace{\frac{\overleftarrow{\partial}}{\partial\eta}\left(\bar{\rho}\frac{V}{J}\right)_{j+\frac{1}{2}}}_{\text{supersonic}} + (1-\theta_{i+1})\underbrace{\frac{\overleftarrow{\partial}}{\partial\eta}\left(\tilde{\bar{\rho}}\frac{V}{J}\right)_{j+\frac{1}{2}}}_{\text{marching subsonic}} \tag{15}$$

where

$$\theta_{i+1} = 1 \quad \text{if} \left(a_{11} - \frac{U^2}{a^2}\right)_{i+1} < 0 \quad \text{(supersonic point)}$$

$$\theta_{i+1} = 0 \quad \text{if} \left(a_{11} - \frac{U^2}{a^2}\right)_{i+1} \geq 0 \quad \text{(MSR)}$$

When $\theta_{i+1} = 1$, that is, the point is *supersonic* with respect to ζ, only the first term in Eq. (15) is used and the biased density $\bar{\rho}$ is defined by (for $V > 0$),

$$\bar{\rho}_{j+\frac{1}{2}} = \left(1 - \bar{\nu}_{j+\frac{1}{2}}\right)\rho^*_{j+\frac{1}{2}} + \tfrac{1}{2}\bar{\nu}_{j+\frac{1}{2}}\left(\rho^*_j + \rho^*_{j-1}\right) \tag{16}$$

where

$$\bar{\nu} = \max\left(0, 1 - a_{22}\frac{a^2}{V^2}\right)$$

In Eq. (16), the evaluation of ρ^* depends on whether the flow is conical or nonconical. For conical flows, all ρ^* quantities are evaluated at the ith plane. For nonconical flows, at each nonconical marching plane, initially ρ^* is set to be the value at the ith plane and then subsequently iterated to convergence by setting ρ^* to the previous iterated value of ρ at the current $i+1$ plane. Reference 5 provides more details on the density biasing procedure and the implicit treatment of $(\overleftarrow{\partial}/\partial\eta)[\bar{\rho}(V/J)]_{j+\frac{1}{2}}$ in Eq. (15).

When the point is *elliptic*, the density biasing is defined by

$$\tilde{\bar{\rho}}^{n+1}_{j+\frac{1}{2}} = \left(1 - \tilde{\bar{\nu}}_{j+\frac{1}{2}}\right)\rho^n_{j+\frac{1}{2}} + \tfrac{1}{2}\tilde{\bar{\nu}}_{j+\frac{1}{2}}\left(\rho^n_j + \rho^n_{j-1}\right) \tag{17}$$

where $\tilde{\bar{\nu}} = \max[0, 1 - (a^2/q^2)]$. As before, the superscript $n+1$ denotes the current relaxation cycle for a subsonic bubble calculation. Note the difference in the definition of $\bar{\nu}$ and $\tilde{\bar{\nu}}$. The density biasing in the cross-flow direction η is turned off when the total velocity q is less than the speed of sound a, just as in the marching ζ direction [Eq. (13)]. The implicit treatment of V in the marching subsonic operator of Eq. (15) is the same as that of the supersonic part, explained in Ref. 5.

A similar procedure is implemented for the $[\rho(W/J)]_\xi$ term in Eq. (1).

Implicit Factorization Algorithm

Combining the various terms of Eq. (1) as represented by Eqs. (10)-(17) together with the terms arising from $[\rho(W/J)]_\xi$ will result in a fully implicit model. This is solved using an approximate factorization implicit scheme. After some rearrangement of the terms, the factored implicit scheme becomes

$$\left[1 + \frac{A_3}{\beta\Delta\zeta}\frac{\partial}{\partial\xi} + \frac{1}{\beta}\frac{\partial}{\partial\xi}\left(\frac{\hat{\rho}}{J}\frac{a_{31}}{\Delta\zeta}\right) + \frac{1}{\beta}\frac{\partial}{\partial\xi}\frac{\hat{\rho}a_{33}}{J}\frac{\partial}{\partial\xi}\right]$$
$$\times\left[1 + \frac{A_2}{\beta\Delta\zeta}\frac{\partial}{\partial\eta} + \frac{1}{\beta}\frac{\partial}{\partial\eta}\left(\frac{\hat{\rho}a_{21}}{J\Delta\zeta}\right) + \frac{1}{\beta}\frac{\partial}{\partial\eta}\frac{\hat{\rho}a_{22}}{J}\frac{\partial}{\partial\eta}\right]\Delta\phi = R \tag{18}$$

The density $\hat{\rho}$ appearing in Eq. (18) can be either $\bar{\rho}$ or $\tilde{\bar{\rho}}$ depending on the sign of $[a_{11} - (U^2/a^2)]$ as illustrated in Eq. (15).

Equation (18) has the form

$$L_\xi L_\eta(\Delta\phi) = R \tag{19}$$

and it is implemented as follows:

$$L_\xi(\Delta\phi)^* = R \qquad L_\eta(\Delta\phi) = (\Delta\phi)^* \qquad \phi_{i+1} = \phi_i + \Delta\phi \tag{20}$$

The various quantities appearing in Eq. (18) are given by

$$\beta = \frac{1}{\Delta\zeta^2}\left[\theta_i A_1 - (1-\theta_{i+1})\frac{\Delta\zeta}{\Delta\zeta_0}\left(\frac{\tilde{\rho}a_{11}}{J}\right)_{i+1}\right]$$

$$A_1 = \frac{\rho_i}{J_{i+1}}\left(a_{11} - \frac{U^2}{a^2}\right)$$

$$A_2 = \theta_i\left[\frac{\rho_i}{J_{i+1}}\left(a_{12} - \frac{UV}{a^2}\right)\right] - (1-\theta_{i+1})\frac{\Delta\zeta}{\Delta\zeta_0}\left(\frac{\tilde{\rho}a_{12}}{J}\right)_{i+1}$$

$$A_3 = \theta_i\left[\frac{\rho_i}{J_{i+1}}\left(a_{13} - \frac{UW}{a^2}\right)\right] - (1-\theta_{i+1})\frac{\Delta\zeta}{\Delta\zeta_0}\left(\frac{\tilde{\rho}a_{13}}{J}\right)_{i+1}$$

$$\Delta\zeta_0 = \zeta_{i+2} - \zeta_{i+1}, \qquad \Delta\zeta = \zeta_{i+1} - \zeta_i \tag{21}$$

and the right-hand side term R consists of various known quantities.

If the flowfield does not contain an embedded MSR or TSR, the implicit factored algorithm of Eq. (18) performs a pure marching procedure starting from an initial known data plane. In this situation, there is no need to go back to the upstream starting plane and iterate the solution. However, if a subsonic bubble is present (between planes AB and CD in Fig. 2), then the solution procedure of Eq. (18) performs a relaxation method and iterates for the elliptic subsonic bubble to converge [superscript n in Eqs. (12), (13), and (17) refers to the relaxation cycle counter].

Initial and Boundary Conditions

Initial Conditions

For a pure supersonic flow, initial conditions need to be prescribed only at the starting plane. Usually, the starting plane is set close to the apex of the configuration to be solved and the conical solutions are prescribed.

Inside an MSR, as in Fig. 2, when Eq. (12) is applied at an $(i+1)$ grid point, information on ϕ_{i+2} is required to form the density $\tilde{\rho}$ and various derivative terms. For the first relaxation pass, an initial estimate for quantities in the $(i+2)$ plane is prescribed in the following manner:

$$\underbrace{\frac{\vec{\partial}}{\partial\zeta}\left(\rho\frac{U}{J}\right)_{i+1}}_{\text{MSR operator}} = \frac{1}{\Delta\zeta_0}\left\{\underbrace{\left(\rho\frac{U}{J}\right)_{i+2}}_{\text{needs initial estimate}} - \left(\frac{\rho}{J}\left(a_{11}\phi_\zeta + a_{12}\phi_\eta + a_{13}\phi_\xi\right)\right)\right\}_{i+1} \tag{22}$$

In Eq. (22), sonic conditions are assumed at $(i+2)$ for the first relaxation pass,

$$\rho_{i+2} = \rho^*, \qquad U_{i+2} = q^*\sqrt{(a_{11})_{i+2}} \tag{23}$$

The sonic values ρ^* and q^* are purely a function of the freestream Mach number M_∞. Also, ρ_{i+1} in Eq. (22) is initialized to be ρ_i.

For the second relaxation cycle and onward $(n \geq 1)$, the conditions from the previous relaxation cycle are used,

$$\left(\rho\frac{U}{J}\right)_{i+2}^{n+1} \doteq \left(\rho\frac{U}{J}\right)_{i+2}^{n}, \qquad \rho_{i+1}^{n+1} \doteq \rho_{i+1}^{n} \tag{24}$$

Boundary Conditions

At a solid boundary, the contravariant velocity V is set to zero. Exact implementation of $V=0$ in the implicit treatment of Eq. (18) is described in Ref. 4.

The outer boundary is set away from the bow shock and the freestream velocity potential ϕ_∞ is imposed along that boundary. All discontinuities in the flowfield are captured. The precise density biasing activator ν, based on the characteristic theory, allows for sharp capturing of shocks in the flow.

Behind the trailing edge of a wing, a wake model is imposed. Figure 4 shows a schematic of a wake model. At a point P lying on the wake, the boundary condition is that there is no jump in the pressure across the wake, i.e., $(p_p - P_Q) = 0$. In the full potential (isentropic) formulation, this translates into the condition that the jump in density $(\rho_p - \rho_Q)$ is zero, or the jump in the total velocity q is zero $[(q_P - q_Q) = 0]$. The jump in q across the wake is set to zero in an approximate manner in the following way.

First, compute the jump in the potential ϕ at the trailing-edge point P' and maintain that jump constant along the line $P'P$ in Fig. 4. At the wake point P, Eq. (1) is not valid. Instead of solving Eq. (1), $\phi_{\eta\eta} = 0$ is satisfied at the wake point P to achieve the condition $(\phi_\eta)_P - (\phi_\eta)_Q = 0$. Incorporating a constant jump in ϕ along $P'P$ insures $(\phi_\zeta)_P - (\phi_\zeta)_Q = 0$. The net effect is that $(q_P - q_Q)$ is approximately set to zero, yielding the necessary wake boundary condition. The following section presents a calculation performed for a realistic wing/body/wake fighter model and shows an excellent matching of the pressures across the wake, using the above wake boundary condition.

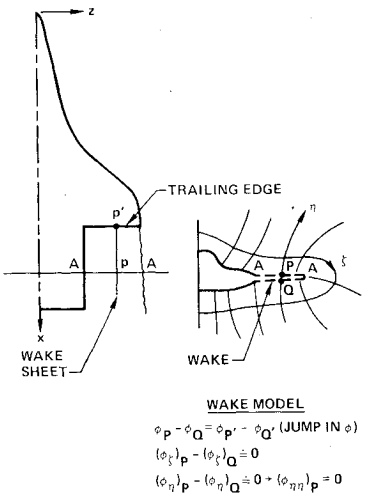

Fig. 4 Wake boundary condition.

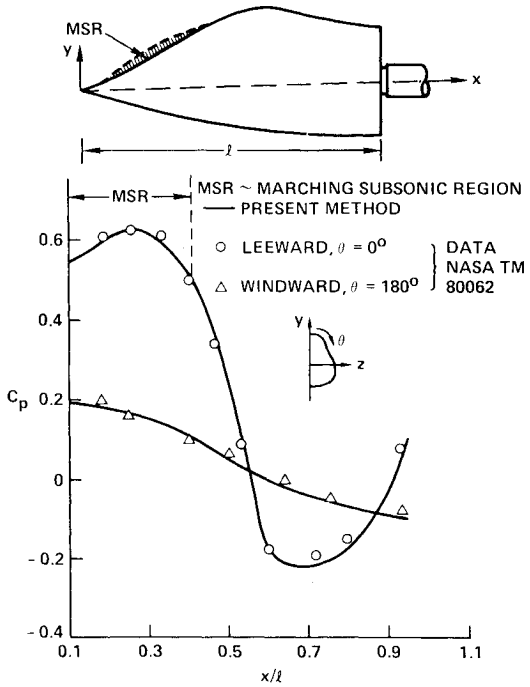

Fig. 5 Axial surface pressure distribution for a developed cross-section forebody ($M_\infty = 1.7$, $\alpha = -5$ deg).

Grid System

The transformation from the physical space (x, y, z) to a body-fitted computational space (ζ, η, ξ) is performed numerically at each constant ζ plane by using the elliptic grid generation technique of Ref. 6. Once the grid is generated, all the metric terms a_{ij} in Eq. (2) and the Jacobian J in Eq. (3) are computed by numerical differentiation. As described in Ref. 5, a freestream error subtraction is performed at each grid point to account for any improper metric cancellation.

Density Biasing Summary

This section summarizes in a tabular form the type-dependent density biasing procedures incorporated in this paper to generate the proper artificial viscosity. See Table 1.

Table 1 Summary to type-dependent density biasing procedure

Term	Total supersonic	Marching subsonic	Total subsonic
Definition	$[a_{11} - (U^2/a^2)] < 0$, $q > a$	$[a_{11} - (U^2/a^2)] > 0$, $q > a$	$[a_{11} - (U^2/a^2)] > 0$, $q < a$
ρU in ζ direction	Upwind differencing, Eq. (11)	Density biasing based on $[1 - (a^2/q^2)]$ in Eq. (13)	Shut off density biasing
$\rho V, \rho W$ in η, ξ directions	Density biasing based on $[1 - a_{22}(a^2/V^2)]$, $[1 - a_{33}(a^2/W^2)]$ $\bar{\rho}$ in Eq. (16)	Density biasing based on $[1 - (a^2/q^2)]$ $\tilde{\rho}$ in Eq. (17)	Shut off density biasing

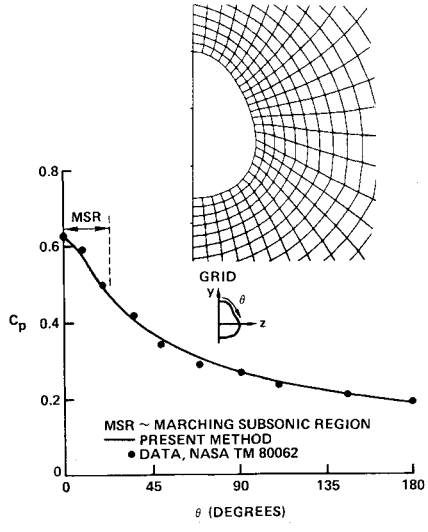

Fig. 6 Circumferential pressure distribution for a developed cross-section forebody ($M_\infty = 1.7$, $\alpha = -5$ deg, $x/l = 0.28$).

IV. Results

As illustrated in Fig. 2, supersonic marching calculations are performed from the nose until an embedded MSR forms. In Fig. 2, the plane AB is the last supersonic marching plane preceding the subsonic bubble and forms the upstream computational boundary for the relaxation calculation. For the first relaxation pass through the subsonic bubble region, θ_{i+1} in Eq. (10) is set equal to θ_i and $(\rho U)_{i+2} = \rho^* q^*$. From the second relaxation cycle on, θ_{i+1}, θ_i, and $(\rho U)_{i+2}$ are computed according to their definitions. A typical supersonic flow with a subsonic bubble calculation required at most only four relaxation cycles (iterating back and forth between planes AB and CD) to obtain a converged location for the bubble. The initial guess, based on the sonic conditions $\rho^* q^*$, worked out very well for all the subsonic bubble cases presented in this paper. The (η, ξ) marching plane can be any arbitrary surface, but for convenience was chosen to be a constant x plane.

The step size in the marching direction ζ for the supersonic part $\{[a_{11} - (U^2/a^2)] < 0,\ q > a\}$ was automatically chosen by setting the Courant number[5] to be around 5. Once the MSR forms, the eigenvalues become complex and the step size cannot be computed based on a specified Courant number. For marching planes containing the MSR/TSR, the step size was specified into the code depending on the geometry variation. When geometry changes were drastic (region of emergence of a wing from a fuselage), usually a smaller step size $\Delta\zeta$ was required (as small as $0.003 \sim 0.005$ for a total length of one) to properly account for rapid changes in the flow. Once the MSR/TSR is fully captured and the flow becomes supersonic again, the step size selection once again becomes based on the Courant number. For a pure supersonic flow all the way, the entire calculation could be performed using 40 planes

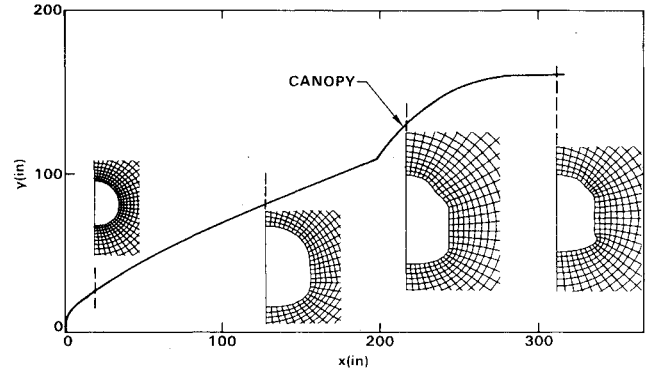

Fig. 7 Nose region geometry for Space Shuttle.

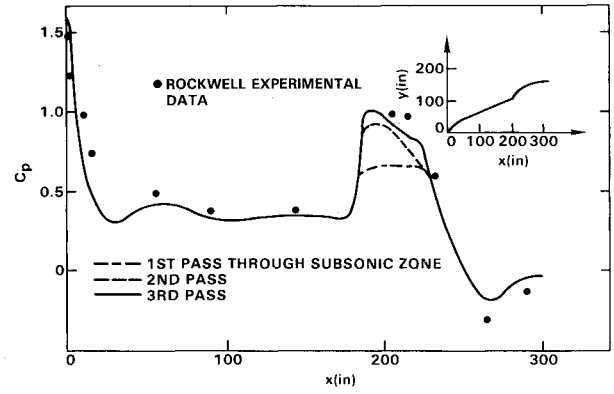

Fig. 8 Surface pressure distribution at leeward plane of symmetry.

or less ($\Delta\zeta > 0.025$). However, once an MSR or TSR is present, the total number of ζ planes in the calculation could go as high as 300.

Figure 5 shows the surface pressure distribution in the axial direction on the upper ($\theta = 0$, lee side) and lower ($\theta = 180$ deg, windward side) plane of symmetry for a developed cross-section forebody geometry reported in Ref. 7. At $M_\infty = 1.7$ and $\alpha = -5$ deg, the lee side has an embedded MSR that required use of the relaxation operator in Eq. (10). A pure supersonic x marching for this case would have failed without the MSR treatment described in this paper.

Figure 6 shows the circumferential pressure distribution for the same developed cross-section forebody at $M_\infty = 1.70$, $\alpha = -5$ deg, and $x/l = 0.28$. The embedded MSR thickness is the largest at this axial station. The extent of the subsonic bubble is marked in Fig. 6. The results of Figs. 5 and 6 exhibit only MSR—TSR is not present.

To simulate both the MSR and TSR, the flow over the Shuttle orbiter at $M_\infty = 1.4$ and $\alpha = 0$ deg was considered. The side view, cross section, and grid in the fuselage/canopy region of the orbiter are shown in Fig. 7. At this Mach

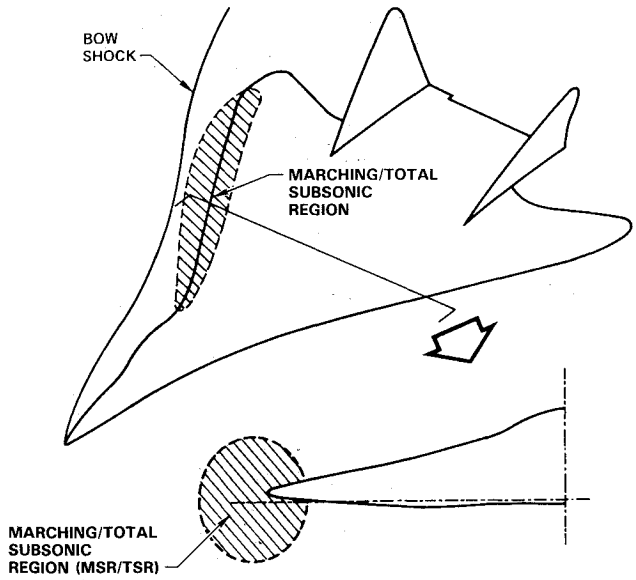

Fig. 9 Supersonic fighter with an embedded marching subsonic region near the leading edge.

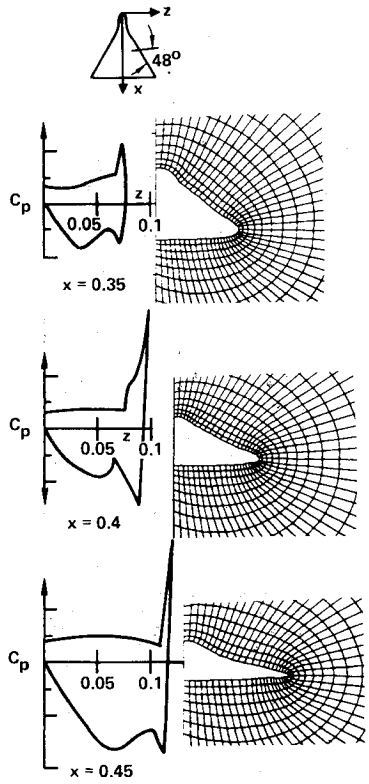

Fig. 10 Pressure distribution on a fighter-like configuration ($M_\infty = 1.6$, $\alpha = 5$ deg).

number, the fuselage/canopy junction exhibits a large MSR/TSR. Figure 8 shows the surface pressure distribution along the leeward plane of symmetry. At $x \cong 4.3$ m (170 in.), which is the beginning of the canopy, the pressure increases rapidly from $C_p \cong 0.3$ to 1.0 and an MSR/TSR is formed. It required three relaxation cycles to develop the solution. The comparison with the Rockwell experimental data is favorable. The blunt body initial solution for this Shuttle case was obtained from the unsteady full potential code of Ref. 8.

Figure 9 shows a supersonic fighter configuration with a wing sweep of around 48 deg. At a freestream Mach number of 1.6 and $\alpha = 5$ deg, the leading edge of the wing exhibits an MSR/TSR. To solve the flowfield over such a fighter configuration, one needs to use the embedded subsonic bubble treatment. Figure 10 shows the surface pressure at various axial stations along with respective grid distribution for the wing/body geometry. For this case, the MSR/TSR starts around $x = 0.4$. Figure 11 shows the pressure distribution for the fighter configuration of Fig. 9 at an axial station $x/l = 0.85$, where a wake sheet is present. The grid distribution goes around the wake sheet just like a wing/body case. The approximate wake model described in the paper seems to provide the correct zero pressure jump condition across the wake, as seen in Fig. 11. Figure 11 shows the simulation without the

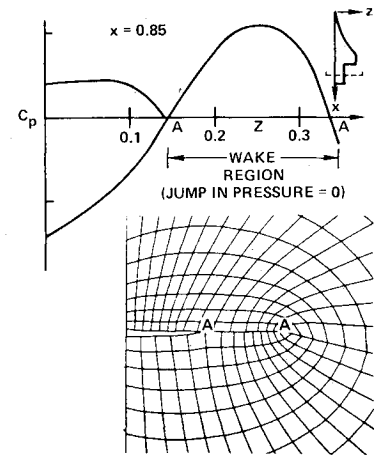

Fig. 11 Grid and pressure distribution in the wake region of a fighter-like configuration ($M_\infty = 1.6$, $\alpha = 5$ deg, $x = 0.85$).

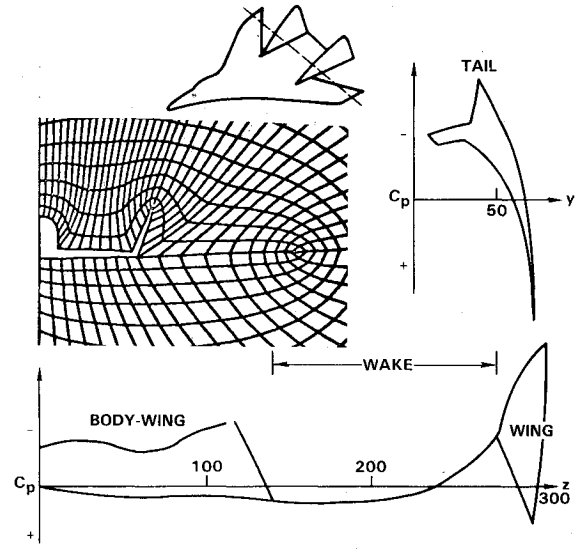

Fig. 12 Circumferential pressure distribution in the vertical tail and wing region of a fighter-like configuration ($M_\infty = 1.6$, $\alpha = 4.46$ deg, $x/l = 0.90$).

Table 2 Test cases for fighter-like configurations

α, deg	5	5	5	5
M_∞	1.6[a]	1.6[b]	1.4[b]	1.6[b]
Λ, deg	48	48	48	55
C_L				
Code	0.298	0.3016	0.3561	0.29186
Data[c]	0.277	0.295	0.342	0.3
C_D				
Code	0.0462	0.04916	0.04117	0.028129
Data[a]	0.0457	0.0493	0.0425	0.0301

[a]Tail off. [b]Tail on. [c]Rockwell data.

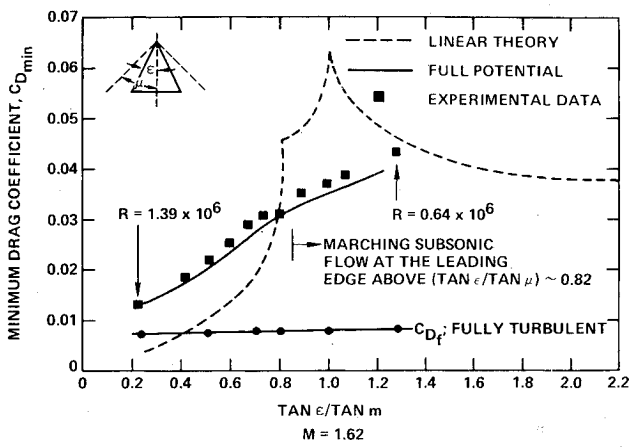

Fig. 13 Drag prediction for a double-wedge delta wing at $M_\infty = 1.62$, $\alpha = 0$ deg; for sweep angles less than 60 deg, the leading edge has a marching subsonic flow ($C_{D_{min}} = C_{D_f} + C_{D_{inviscid}}$).

vertical tails. Figure 12 shows the result for a different fighter model with a pronounced wing/body shape and a vertical tail. At this cross section, $x/l = 0.9$, the geometry is multiply connected with a wake sheet present between the tail and the wing. The circumferential pressure distribution on the wing/body/tail/wake and the gridding are shown in Fig. 12.

The lift and drag coefficients from the present calculation for a fighter model are given in Table 2. The comparison with Rockwell experimental data is excellent.

Figure 13 shows the drag prediction capability of the full potential code by demonstrating it on a double-wedge delta wing at $M_\infty = 1.62$. At this Mach number, the leading edge exhibited the presence of an MSR for sweep angles less than 60 deg. A pure supersonic marching code would not have worked for this case. The drag calculation from the full potential code compared very well with the experimental data available in the Princeton series.

V. Conclusions

A nonlinear full potential method has been developed to treat supersonic flows with embedded subsonic regions. A conservative switching scheme is employed to transition from the supersonic marching algorithm to a subsonic relaxation procedure. The theory of characteristic signal propagation plays a key role in activating various density biasing procedures to produce the necessary artificial viscosity. The method has been shown to produce results that were hitherto not possible using a pure supersonic marching scheme. The concept of density biasing will be modified in the future to a flux biasing procedure described in the Appendix.

Appendix: Flux Biasing Procedure

Based on the work of Hafez et al.,[9] it is possible to modify the density biasing concept to a flux biasing procedure.

Consider the term $(\partial/\partial\eta)[\tilde{\rho}(V/J)]$ in Eq. (15). The density biasing procedure defines $\tilde{\rho}$ to be

$$\tilde{\tilde{\rho}}_{j+\frac{1}{2}} = (1-\nu)\rho_{j+\frac{1}{2}} + \tfrac{1}{2}\nu(\rho_j + \rho_{j-1}) \tag{A1}$$

where

$$\nu = \max\left[0, 1-(a^2/q^2)\right]$$

In the flux biasing technique, it will be modified to

$$\frac{\overleftarrow{\partial}}{\partial\eta}\left(\tilde{\rho}\frac{V}{J}\right)_{j+\frac{1}{2}} = \frac{\overleftarrow{\partial}}{\partial\eta}\left[\frac{V}{Jq}\left\{\rho q - \Delta\eta\,\overleftarrow{\partial}_\eta(\rho q)_-\right\}\right]_{j+\frac{1}{2}} \tag{A2}$$

where

$$(\rho q)_- = 0 \qquad \text{if } q \le a$$
$$= (\rho q) - \rho^* q^* \qquad \text{if } q > a,$$

where ρ^* and q^* represent sonic conditions, a the local speed of sound, and (ρq) the flux. When the flow is purely subsonic, the flux biasing is turned off automatically.

Acknowledgment

This work was partially supported by NASA-Langley Research Center under Contract NAS1-15820.

References

[1]Jameson, A., "Transonic Potential Flow Calculations using Conservation Form," *AIAA Second Computational Fluid Dynamics Conference Proceedings*, AIAA, New York, 1975, pp. 148-155.

[2]Holst, T.L., "Fast, Conservative Algorithm for Solving the Transonic Full Potential Equation," *AIAA Journal*, Vol. 18, Dec. 1980, pp. 1431-1439.

[3]Siclari, M.J., "Computation of Nonlinear Supersonic Potential Flow over Three-Dimensional Surfaces," AIAA Paper 82-0167, Jan. 1982.

[4]Shankar, V., "A Conservative Full Potential, Implicit, Marching Scheme for Supersonic Flows," *AIAA Journal*, Vol. 20, Nov. 1982, pp. 1508-1514.

[5]Shankar, V. and Osher, S., "An Efficient Full Potential Implicit Method Based on Characteristics for Analysis of Supersonic Flows," *AIAA Journal*, Vol. 21, Sept. 1983, pp. 1262-1270.

[6]Shankar, V., Rudy, S., and Szema, K.-Y., "Application of a Two-Dimensional Grid Solver for Three-Dimensional Problems," *ASME Applied Mechanics, Bioengineering, and Fluids Engineering Conference*, Vol. No. G00222, ASME, New York, June 1983.

[7]Townsend, J.C., Howell, D.T., Collins, I.K., and Hayes, C., "Surface Pressure Data on a Series of Analytic Forebodies at Mach Numbers from 1.7 to 4.50 and Combined Angles of Attack and Sideslip," NASA TM 80062, June 1979.

[8]Shankar, V., "Implicit Treatment of the Unsteady Full Potential Equation in Conservation Form," AIAA Paper 84-0262, Jan. 1984.

[9]Hafez, M., Osher, S., and Whitlow, W. Jr., "Improved Finite Difference Schemes for Transonic Potential Calculations," AIAA Paper 84-0092, Jan. 1984.